DALTON
FULL PAPER

The reactivity of dibenzotetramethyltetraaza[14]annulene-Mn(II): functionalisation of manganese in a macrocyclic environment

Federico Franceschi,[a] Joëlle Hesschenbrouck,[a] Euro Solari,[a] Carlo Floriani,*[a] Nazzareno Re,[b] Corrado Rizzoli[c] and Angiola Chiesi-Villa[c]

[a] *Institut de Chimie Minérale et Analytique, BCH, Université de Lausanne, CH-1015 Lausanne, Switzerland. E-mail: carlo.floriani@icma.unil.ch*
[b] *Facoltà di Farmacia, Università degli Studi "G. D'Annunzio", I-66100 Chieti, Italy*
[c] *Dipartimento di Chimica, Università di Parma, I-43100 Parma, Italy*

Received 11th October 1999, Accepted 30th November 1999

The present report deals with the one electron oxidation and the one- and two-electron reduction of [Mn(tmtaa)L], [L = THF, **1a**; L = none, **1b**; tmtaa = dibenzotetramethyltetraaza[14]annulene]. The former class of reactions led to the formation of a variety of functionalised Mn(III) species, [(tmtaa)Mn–X] [X = I, **2**; X = Cl, **3**; X = NCS, **5**], including the cationic derivatives [Mn(tmtaa)(L)(L′)]BPh_4 [L = L′ = THF, **4a**; L = L′ = DME, **4b**; L = Py, L′ = none, **4c**]. The magnetic properties of the Mn(III) derivatives are strongly dependent on the axial ligand. Reaction of **1a** with NO gave [(tmtaa)Mn(NO)], **6**, which takes up an axial pyridine leading to the diamagnetic [(tmtaa)Mn(NO)-(Py)], **7**. Complex **6** displays a peculiar magnetic behavior, which has been interpreted as a $S = 0 \rightleftharpoons S = 2$ spin equilibrium with a $\Delta H_{eff} = 4.0$ kJ mol^{-1} and a $\Delta S_{eff} = 11.3$ J mol^{-1} K^{-1} associated to the spin transition process. Reaction of **1** with sodium metal in DME leads to $[Mn_2(\mu_2\text{-tmtaa})_2\{Na\cdot(DME)_2\}_2]$, **8**, while in THF $[Mn_2(\text{*tmtaa}_2\text{*})Na_4\cdot(THF)_6]$, **9**, is formed. Extended Hückel calculations have been performed for a better understanding of the magnetic and electronic properties of **6** and **9**. The proposed structures have been supported by X-ray analyses of **3**, **4b**, **6**, **8**, and **9**.

Introduction

Although the redox chemistry of Mn(II) is a field of interest in coordination chemistry,[1] an extensive synthetic study on its redox behavior in a macrocyclic environment has surprisingly been poorly explored. The single aspect which has recently been intensely investigated is the redox behavior of Mn-porphyrin and Mn-Schiff base derivatives, as far as concerns their catalytic activity towards oxygen transfer processes.[2–5] The other aspect which has been relatively neglected is the magnetic analysis and interpretation of the various Mn(II), Mn(III), and Mn(IV) in a macrocyclic environment. The present report focuses on the redox properties of the dibenzotetramethyltetraaza[14]annulene-Mn(II), with particular emphasis on the synthetic results, and the magnetic and theoretical analysis of the Mn(II) and Mn(III) derivatives. The only precedent of the chemistry we are reporting here is the synthesis of [Mn(tmtaa)·(NEt_3)],[6] though its reported synthesis is not suitable for studying the reactivity. In addition to a novel synthesis of the parent compound [Mn(tmtaa)·(THF)], here we report its transformation into Mn(III) derivatives [Mn(tmtaa)X] [X = Cl, I, NCS], the reaction with NO leading to a paramagnetic and to a diamagnetic nitrosyl derivative, and the ligand-reduced form $[Mn^{II}_2(\text{*tmtaa}_2\text{*})]^{4-}$, where the two tmtaa units are bridged by two C–C bonds (see Chart 1B for the structure of $\text{*tmtaa}_2\text{*}$) and the two manganese ions experience a very close proximity [Mn···Mn, 2.569(2) Å].

Experimental

General

All reactions were carried out under an atmosphere of purified nitrogen. Solvents were dried and distilled before use by standard methods. Infrared spectra were recorded with a Perkin-Elmer FT 1600 spectrophotometer; NMR and X-band ESR spectra were recorded respectively by DPX-400 and ECS-106 Bruker spectrometers. $[Mn_3Mes_6]$·tol[7] (Mes = 1,3,5-trimethylbenzene, tol = toluene), tmtaaH_2,[8] and tmtaaLi_2[9] were prepared according to published procedures. Magnetic susceptibility measurements were made with a Quantum Design MPMS5 SQUID susceptometer operating at a magnetic field strength of 1 kOe. Corrections were applied for diamagnetism calculated from Pascal constants.[10] Effective magnetic moments were calculated as $\mu_{eff} = 2.828(\chi_{Mn}T)^{1/2}$, where χ_{Mn} is the magnetic susceptibility *per* manganese. Fitting of the magnetic data to the theoretical expression were performed by minimising the agreement factor, defined as $\Sigma \frac{[\chi_i^{obsd}T_i - \chi_i^{calcd}T_i]^2}{(\chi_i^{obsd}T_i)^2}$ through a Levenberg–Marquardt routine.

Syntheses

Compound 1a. The ligand tmtaaH_2 (15.3 g; 44.5 mmol) was added to a THF (400 cm^3) solution of $[Mn_3Mes_6]$·tol (14.3 g; 14.8 mmol). The resulting orange-brown suspension was stirred for 3 h, then was concentrated to half of its initial volume and *n*-hexane (150 cm^3) was added. The dark-red microcrystalline product was collected and dried *in vacuo* (17.4 g; 83%) (Found C, 66.59; H, 6.32; N, 11.61. **1a**, $C_{26}H_{30}MnN_4O$ requires C, 66.52; H, 6.44; N, 11.93%. IR (Nujol, ν_{max}/cm^{-1}): 1538s, 1282m, 1195s, 1115w, 1026m, 938w, 823m, 751s, 708m, 613w, 518w.

Compound 1b. $MnCl_2\cdot(THF)_{1.5}$[11] (12.2 g; 52.2 mmol) was added to a toluene (400 cm^3) solution of tmtaaLi_2 (18.6 g; 52.2 mmol). The resulting orange-brown suspension was stirred for 3 h, then the orange microcrystalline product was separated from LiCl by extraction with mother liquor. *n*-Hexane (150 cm^3) was added and Mn(tmtaa) **1b** was collected and dried *in vacuo* (13.2 g; 64%). (Found C, 65.61; H, 5.73; N, 13.97. **1b**, $C_{22}H_{22}MnN_4$ requires C, 65.50; H, 5.58; N, 14.10%).

Compound 2. A THF (50 cm^3) solution of I_2 (0.38 g; 1.50 mmol) was added to a THF (150 cm^3) suspension of **1a** (1.42 g; 3.02 mmol), previously cooled to −30 °C. The resulting brown suspension was allowed to reach room temperature and was stirred overnight. A brown-red microcrystalline solid was collected and dried *in vacuo* (1.13 g; 63%). (Found: C, 52.41; H, 5.18; N, 9.21. **2**·THF, $C_{26}H_{30}IMnN_4O$ requires C, 52.36; H, 5.07; N, 9.39%). IR (Nujol, ν_{max}/cm^{-1}): 1576w, 1546s, 1517s, 1427s, 1194w, 1030m, 949w, 847w, 761s, 715w, 530w.

Compound 3. $HgCl_2$ (1.10 g; 4.79 mmol) was added to a THF (300 cm^3) suspension of **1a** (1.90 g; 4.05 mmol) to give a black suspension that was stirred overnight. The solid was extracted with the mother liquor resulting in a black crystalline product, which was collected and dried *in vacuo* (1.78 g; 74%). Crystals suitable for X-ray analysis were grown in a pyridine solution chilled to 5 °C and contain pyridine of crystallisation, **3**·1.5Py. (Found: C, 61.65; H, 5.81; N, 10.97. **3**·THF, $C_{26}H_{30}ClMnN_4O$ requires C, 61.85; H, 5.99; N, 11.10%). IR (Nujol, ν_{max}/cm^{-1}): 1530s, 1276m, 1193m, 1121w, 1063s, 1033s, 941w, 911w, 848w, 757s, 668w, 632w, 531w.

Compound 4. $NaBPh_4$ (2.43 g, 7.10 mmol) was added to a THF (300 cm^3) suspension of **3**·(THF) (3.59 g, 7.10 mmol) and the mixture was refluxed for 2 h. NaCl was filtered off, the solution was evaporated to dryness and a suspension of the residue was prepared in *n*-hexane (125 cm^3). The black solid was collected and dried *in vacuo* (4.89 g; 80%). (Found: C, 75.48; H, 6.85; N, 6.42. **4a**, $C_{54}H_{58}BMnN_4O_2$ requires C, 75.35; H, 6.79; N, 6.51%). IR (Nujol, ν_{max}/cm^{-1}): 1944w, 1883w, 1817w, 1772w, 1579m, 1529s, 1261m, 1188w, 1123w, 1030s, 939w, 859m, 762m, 708m, 610m, 536w, 471w. Crystals suitable for X-ray analysis were grown at room temperature in a saturated DME solution, and obtained as **4b**. The pyridine-solvated **4c** was prepared as follows: **4a** (2.47 g; 2.87 mmol) was dissolved in THF (200 cm^3) and pyridine (0.23 cm^3; 2.87 mmol) was added. The black solution was stirred for 30 min before it was taken to dryness. The residue was suspended and washed in hexane (200 cm^3) and the product was collected and dried *in vacuo* (2.13 g; 93%). (Found: C, 76.82; H, 5.85; N, 8.71. **4c**, $C_{51}H_{47}BMnN_5$ requires C, 76.98; H, 5.95; N, 8.80).

Compound 5. A suspension of **3**·(THF) (1.10 g; 2.18 mmol) was prepared in a mixture of methanol (90 cm^3) and water (10 cm^3). NH_4NCS (170 mg; 2.18 mmol) was added and the black suspension was stirred overnight before a black microcrystalline product was collected and dried *in vacuo* (0.96 g; 91%). (Found: C, 58.97; H, 4.98; N, 14.30. **5**·MeOH, $C_{24}H_{26}MnN_5OS$ requires C, 59.13; H, 5.38; N, 14.37%). IR (Nujol, ν_{max}/cm^{-1}): 2053s, 1576w, 1525s, 1432s, 1261s, 1010s, 937m, 843m, 793m, 753s 529w.

Compound 6. NO was allowed to diffuse slowly into a flask where a THF (130 cm^3) suspension of **1a** (2.36 g; 5.03 mmol) was being stirred. After 24 h a black microcrystalline product was collected and dried *in vacuo* (1.03 g; 41%). Crystals suitable for X-ray analysis were grown at room temperature in a saturated THF solution. (Found: C, 62.35; H, 6.04; N, 13.92. **6**·THF, $C_{26}H_{30}MnN_5O_2$ requires C, 62.52; H, 6.05; N, 14.02%). IR (Nujol, ν_{max}/cm^{-1}): 1685s, 1577m, 1532s, 1281w, 1196m, 1061w, 1032m, 796w, 752m.

Compound 7. **6**·THF (1.40 g; 2.80 mmol) was dissolved in pyridine (30 cm^3) and the brown solution was stirred for 30 min. Et_2O (100 cm^3) was added and the suspension was allowed to stand for 3 h at 5 °C before a dark-orange microcrystalline product was collected and dried *in vacuo* (1.25 g; 88%). (Found: C, 63.92; H, 5.39; N, 16.77. **7**, $C_{27}H_{27}MnN_6O$ requires C, 64.03; H, 5.37; N, 16.59%). ^{1}H NMR (400 MHz, pyridine-d_5, 298 K): δ 6.52 (br s, 2H, Ar); 6.24 (br s, 2H, Ar); 2.80 (s, 1H, CH); 1.82 (s, 6H, CH_3). ^{13}C NMR (100.6 MHz, pyridine-d_5, 298 K): δ 163.5 (C=N); 160.3 (C_{quat} Ar); 123.1 (CH Ar); 120.2 (CH Ar); 119.4 (CH); 20.6 (CH_3). IR (Nujol, ν_{max}/cm^{-1}): 1700s, 1600w, 1567w, 1544s, 1427s, 1409s, 1353s, 1191s, 1069w, 1033m, 1017m, 736s, 700m, 649w, 620w, 582w.

Compound 8. Sodium sand (0.14 g; 5.96 mmol) was added to a DME (200 cm^3) suspension of **1a** (2.80 g; 5.96 mmol). The mixture was stirred overnight to give a dark-orange solution that was taken to dryness. The residue was suspended and stirred in hexane (100 cm^3), then the brown product was collected and dried *in vacuo* (2.93 g; 82%). Crystals suitable for X-ray analysis were grown at room temperature in a saturated diethyl ether solution and contain partial Et_2O of crystallisation around Na. The solvation degree of the crystals is in agreement with the formula $[Mn_2(tmtaa)_2Na_2(Et_2O)_3(DME)]$ (Found C, 60.05; H, 6.90; N, 9.62. **8**, $C_{30}H_{41}MnN_4NaO_4$ requires C, 60.09; H, 6.89; N, 9.34%). IR (Nujol, ν_{max}/cm^{-1}): 1556s, 1527s, 1498s, 1266s, 1175s, 1121m, 1082s, 1014s, 916w, 857w, 791w, 742s, 727s, 696m, 534w, 525w.

Compound 9. Sodium sand (1.04 g; 45.1 mmol) was added to a THF (500 cm^3) suspension of **1a** (10.58 g; 22.5 mmol). The mixture was stirred overnight to give an orange solution that was taken to dryness. A suspension of the residue was prepared and stirred in *n*-hexane (400 cm^3), then the brown product was collected and dried *in vacuo* (12.93 g; 87%). Crystals suitable for X-ray analysis were grown at room temperature in a THF–hexane 1:2 solution. (Found: C, 62.10; H, 6.46; N, 8.78. **9**, $C_{34}H_{46}MnN_4Na_2O_3$ requires C, 61.90; H, 7.03; N, 8.49%). IR (Nujol, ν_{max}/cm^{-1}): 1541s, 1248s, 1169w, 1108w, 1048m, 900w, 734m.

X-Ray crystallography

Suitable crystals were mounted in glass capillaries and sealed under nitrogen. Crystal data and details associated with data collection are given in Table 1. Data for **3**, **4b**, **6**, and **8** were collected on a Rigaku AFC6S single-crystal diffractometer at 298 K for **2** and at 143 K for **4b**, **6**, and **8**. Data reduction was carried out using the Texsan crystallographic software package.[12] Data for **9** were collected on a Mar345 imaging plate system at 223 K. The diffraction data were indexed and processed using the DENZO/HKL suite of programs.[13]

The crystal quality was tested by ψ scans showing that crystal absorption effects could not be neglected for **3**, **4b**, and **6**. The data were corrected for absorption using a semiempirical method.[14]

The function minimized during the least-square refinements was $\Sigma w(\Delta F^2)^2$. Anomalous scattering corrections were included in all structure factor calculations.[15b] Scattering factors for neutral atoms were taken from ref. (15*a*) for nonhydrogen atoms and from ref. (16) for H. Structure solutions were based on the observed reflections [$I > 2\sigma(I)$] while the refinements were based on the unique reflections having $I > 0$ for **3**, **4b**, **6**, and **8**, and $I > 2\sigma(I)$ for **9**. The structures were solved by the heavy-atom method starting from a three-dimensional Patterson map.[17] Refinements were done by full matrix least-squares first isotropically and then anisotropically for all non-H atoms except for the disordered atoms. For all complexes the hydrogen atoms of complexes were put in geometrically calculated positions and introduced in the refinements as fixed atoms contributions (U_{iso} = 0.08 Å^2 for **3**, **6**, **8**, **9**; and 0.05 Å^2 for **4b**, respectively). In the last stage of refinement the weighting

Table 1 Experimental data for the X-ray diffraction studies on crystalline complexes **3**, **4b**, **6**, **8**, and **9**

Complex	**3**[a]	**4b**[b]	**6**[c]	**8**[d]	**9**[e]
Formula	$C_{22}H_{22}ClMnN_4\cdot$ 1.5 C_5H_5N	$C_{30}H_{42}MnN_4O_4\cdot$ $C_{24}H_{20}B$	$C_{22}H_{22}MnN_5O\cdot$ C_4H_8O	$C_{60}H_{82}Mn_2N_8Na_2O_5$	$C_{68}H_{92}Mn_2N_8Na_4O_6$
Formula weight	551.5	896.9	499.5	1151.2	1319.4
a/Å	12.828(3)	12.260(2)	10.892(2)	10.593(3)	14.640(3)
b/Å	13.487(3)	16.785(2)	13.884(2)	19.228(5)	15.823(3)
c/Å	9.040(6)	11.637(1)	16.057(2)	15.663(5)	16.375(3)
α/°	92.49(2)	99.11(2)			97.72(3)
β/°	105.25(2)	91.60(2)	103.89(1)	107.71(3)	102.28(3)
γ/°	61.77(2)	81.55(2)			101.94(3)
V/Å^3	1323.4(6)	2338.8(5)	2357.2(6)	3039.1(16)	3562.6(14)
T/°C	298	143	143	143	223
Space group	$P\bar{1}$ (no. 2)	$P\bar{1}$ (no. 2)	$P2_1/c$ (no. 14)	$P2_1/n$ (no. 14)	$P\bar{1}$ (no. 2)
Z	2	2	4	2	2
μ/cm^{-1}	52.44	26.78	48.34	4.62	4.14
Total reflections measured	5213	8081	4388	7570	21769
Unique total reflections	4973	7633	3961	6977	11988
R(int)	0.041	0.144	0.109	0.085	0.054
N-refinement	4259	6729	3290	5158	7849
R	0.064	0.074	0.085	0.064	0.077
wR_2	0.201	0.229	0.263	0.206	0.219

[a] Complex **3**. One pyridine solvent molecule was found to lie about a centre of symmetry, imposing the nitrogen atom to be statistically distributed over two positions. The nitrogen atom could not be established unambiguously, however. The hydrogen atoms associated with the centrosymmetric pyridine molecule were ignored. [b] Complex **4b**. Refinement of complex **4b** was carried out straightforwardly. [c] Complex **6**. Some carbon atoms of the THF solvent molecule showed rather high thermal parameters suggesting the presence of disorder, which was solved by splitting the C(24) and C(25) atoms over two positions (called A and B) isotropically refined with site occupation factors of 0.5. [d] Complex **8**. One coordination site around the sodium cation was found to be statistically occupied by DME and Et_2O molecules in a 1 : 1 ratio, the molecules approximately sharing the terminal C(27) methyl carbon atoms. The O(2), O(3), C(27), C(28)A, C(29)A, C(30)A (for the DME molecule) and O(4), C(27), C(28)B, C(29)B, C(30)B (for the Et_2O molecule) atoms were then isotropically refined with site occupation factors of 0.5. During the refinement the C–O and C–C bond distances were constrained to be 1.48(1) and 1.54(1) Å, respectively. [e] Complex **9**. Some disorder affected the THF molecules bonded to the Na(2). The best fit was obtained by splitting the C(28), C(29) atoms (molecule A) and C(27), C(28), C(29) atoms (molecule B) over two positions (called A, C and B, D for molecule A and B, respectively) isotropically refined with site occupation factors of 0.5. During the refinement C–C bond distances were constrained to be 1.54(1) Å.

scheme $w = 1/[\sigma^2(F_o^2) + (aP)^2]$ (with $P = (F_o^2 + 2F_c^2)/3$) was applied with a resulting in the value of 0.1255, 0.1552, 0.1481, 0.1069, 0.1647 for **3**, **4b**, **6**, **8**, and **9** respectively. For all complexes the final difference maps showed no unusual features, with no significant peaks above the general background.

All calculations were performed by using SHELXL93[18] implemented on a QUANSAN personal computer equipped with an INTEL PENTIUM II processor.

CCDC reference number 186/1759.

See http://www.rsc.org/suppdata/dt/a9/a908121f/ for crystallographic files in .cif format.

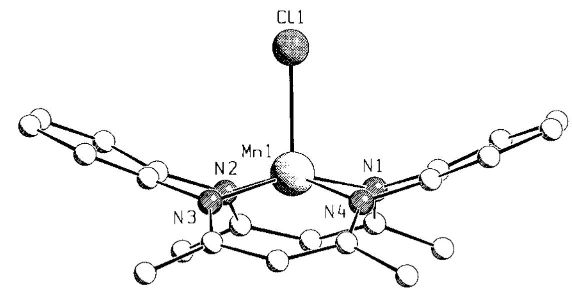

Fig. 1 A SCHAKAL[40] view of complex **3**.

Results and discussion

A Synthetic and structural studies

The synthesis of [Mn(tmtaa)·(THF)] (complex **1a** in Scheme 1) was performed by reacting the ligand in the protic form with Mn_3Mes_6. In THF, the reaction produces the complex free of any salt and particularly of halide ions, which can remain bound to the metal. The alternative synthesis (see Experimental section) from $MnCl_2\cdot(THF)_{1.5}$ and the lithium salt tmtaaLi_2 in toluene led to **1b**, which does not contain any axial ligand at the metal. Such a synthesis is also practicable, but a slow extraction in hot toluene to remove LiCl from the product is required. The complex [Mn(tmtaa)·(NEt_3)] has been previously characterised,[6] though in the present reactivity study we currently use complex **1** as starting material for two basic reasons: i) the published procedure is not suitable for a multi-gram scale preparation; ii) the presence of (NEt_3) coordinated to the metal centre is undesired for a redox reactivity study. The access to a variety of Mn(III) functionalities requires in the first place the preparation of the halide derivatives. The oxidation of **1** has been performed using both iodine or $HgCl_2$ and leads to **2** and **3**, respectively. The formation of the chloride derivative is accessible only using a mild oxidising and chlorinating agent, such as $HgCl_2$. The structure proposed for **3** (see below) has been confirmed by X-ray analysis (Fig. 1).

Selected bond distances and angles for all complexes are quoted in Table 2. Relevant conformational parameters within the [Mn(tmtaa)] moieties are given in Table 3. The labeling scheme adopted for the tmtaa ligand is depicted in Chart 1A.

In complex **3** manganese is in a square pyramidal environment, the metal being displaced by 0.426(2) Å from the planar N_4 core (Table 3). The Mn–Cl vector forms a dihedral angle of 1.5(1)° with the normal to the N_4 core. The tmtaa ligand shows the usual saddle shape conformation.[19] The five-membered chelation rings are folded along the N···N lines (for dihedral angles see Table 3), the metal being displaced by 0.820(2) and 0.868(2) Å from the mean planes through the N(1),C(22), C(17),N(4) and N(2),C(6),C(11),N(3) atoms respectively. The six-membered chelation rings are slightly folded along the N···N lines, the dihedral angles Mn,N(1),N(2) ∧ N(1), C(2),C(3),C(4),N(2) and Mn,N(3),N(4) ∧ N(3),C(13),C(14), C(15),N(4) being 15.1(3)° and 11.7(2)° respectively.

The Mn–Cl ionisation was easily achieved by adding $NaBPh_4$ to a THF suspension of **3**. Manganese(III) in the cationic form, unlike the neutral one, can achieve either the penta- or the

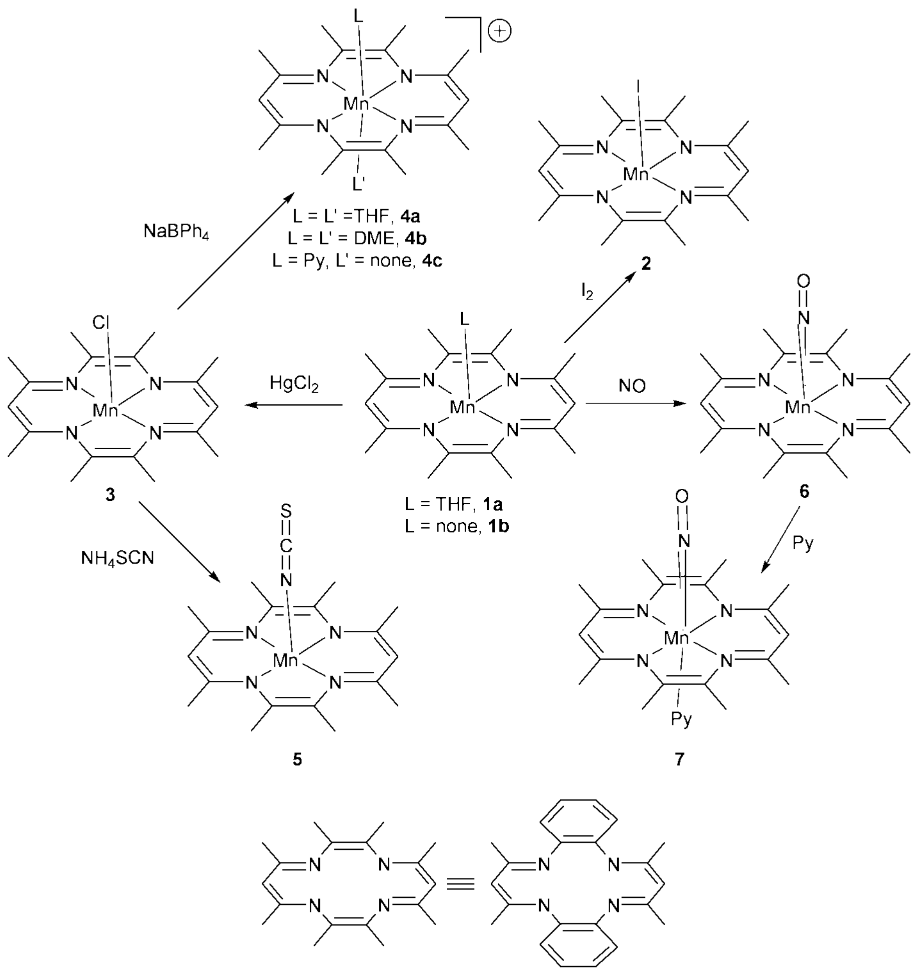

Scheme 1

Table 2 Selected bond distances (Å) and angles (°) for complexes **3**, **4b**, **6**, **8**, and **9**

3							
Mn–N(1)	1.957(4)	Mn–N(3)	1.962(5)	Mn–Cl(1)	2.363(3)		
Mn–N(2)	1.961(5)	Mn–N(4)	1.963(5)				
4b							
Mn–N(1)	1.925(5)	Mn–N(3)	1.929(5)	Mn–O(1)	2.315(4)		
Mn–N(2)	1.927(4)	Mn–N(4)	1.938(4)	Mn–O(3)	2.458(4)		
6							
Mn–N(1)	1.964(6)	Mn–N(3)	1.935(6)	Mn–N(5)	1.612(8)	Mn–N(5)–O(1)	174.9(6)
Mn–N(2)	1.934(7)	Mn–N(4)	1.962(7)	O(1)–N(5)	1.208(11)		
8							
Mn–N(1)	2.110(4)	Mn–N(3)	2.128(6)	Mn–C(1)′	2.234(6)		
Mn–N(2)	2.089(6)	Mn–N(4)	2.108(5)				
9							
	Molecule A	Molecule B		Molecule A	Molecule B		
Mn–N(1)	2.274(5)	2.336(5)	N(3)–C(13)	1.388(7)	1.391(9)		
Mn–N(1)″	2.133(5)	2.186(4)	N(4)–C(15)	1.489(7)	1.491(6)		
Mn–N(2)	2.161(5)	2.124(5)	C(2)–C(15)″	1.699(8)	1.671(9)		
Mn–N(3)	2.143(4)	2.162(6)	C(2)–C(3)	1.521(9)	1.536(9)		
Mn–N(4)	2.319(5)	2.257(5)	C(3)–C(4)	1.349(9)	1.336(10)		
Mn–N(4)″	2.208(4)	2.130(5)	C(13)–C(14)	1.353(10)	1.351(9)		
N(1)–C(2)	1.490(7)	1.483(8)	C(14)–C(15)	1.524(8)	1.530(10)		
N(2)–C(4)	1.398(9)	1.402(6)					

Symmetry transformations used to generate equivalent atoms: ′ $-x, -y, 1-z$; ″ $-x, -y, -z$ and $1-x, 1-y, 1-z$ for molecule A and B, respectively.

hexa-coordination by adding axial ligands (see **4a**, **4b**, and **4c** in Scheme 1). The structure of **4b** is shown in Fig. 2.

The metal is located in an elongated octahedron, with the metal displaced by 0.103(1) Å from the mean plane through the equatorial N_4 core which shows little but significant tetrahedral distortion (Table 3). The mean O(1)–Mn–O(3) line forms a

Table 3 Comparison of relevant conformational parameters within the Mn(tmtaa) moiety for complexes **3**, **4b**, **6**, **8**, and **9**

	3	**4b**	**6**	**8**	**9**	
					Molecule A	Molecule B
(a) Distances (Å) of atoms from the N_4 mean plane[a]						
N(1)	0.015(5)	−0.038(4)	0.018(7)	−0.020(5)	−0.058(5)	0.034(5)
N(2)	−0.015(5)	0.039(4)	−0.018(7)	0.021(5)	0.057(5)	−0.034(5)
N(3)	0.015(5)	−0.038(4)	0.022(7)	−0.021(5)	−0.056(5)	0.038(5)
N(4)	−0.015(5)	0.038(4)	−0.021(7)	0.021(5)	0.057(5)	−0.035(5)
Mn(1)	0.426(2)	0.103(1)	0.448(2)	0.832(2)	0.868(2)	0.864(1)
(b) Dihedral angles (°) between significant planes[b]						
$N_4 \wedge N(1)C_3N(2)$	146.7(2)	151.1(1)	153.4(3)	161.1(2)	168.2(2)	172.8(1)
$N_4 \wedge N(3)C_3N(4)$	149.9(2)	153.2(2)	151.0(3)	161.6(2)	172.5(2)	169.1(2)
$N_4 \wedge N(1)C_6N(4)$	159.7(1)	155.5(1)	160.7(1)	154.9(1)	95.1(1)	95.3(1)
$N_4 \wedge N(2)C_6N(3)$	157.5(1)	154.4(1)	159.4(1)	156.3(1)	172.2(7)	172.5(1)
$N(1)C_3N(2) \wedge N(3)C_3N(4)$	116.3(3)	124.4(2)	124.4(3)	142.8(2)	166.7(3)	166.5(3)
$N(1)C_6N(4) \wedge N(2)C_6N(3)$	137.2(1)	129.9(1)	140.1(1)	131.2(1)	92.4(1)	92.2(1)
$C(6)\cdots C(11) \wedge C(17)\cdots C(22)$	133.4(2)	125.2(2)	135.5(3)	126.6(3)	93.0(2)	92.5(2)

[a] N_4 refers to the least-squares mean plane defined by the N(1), N(2), N(3), N(4) nitrogen atoms. [b] $N(1)C_3N(2)$, $N(3)C_3N(4)$, $N(1)C_6N(4)$, $N(2)C_6N(4)$, $N(2)C_6N(3)$ refer to the least-squares mean plane through atoms N(1),C(2),C(3),C(4),N(2); N(3),C(13),C(14),C(15),N(4); N(4),C(17),C(18),C(19),C(20),C(21),C(22),N(1); and N(2),C(6),C(7),C(8),C(9),C(10),C(11),N(3), respectively. $C(6)\cdots C(11)$ and $C(17)\cdots C(22)$ refer to the planes through the aromatic rings.

(A)

(B)

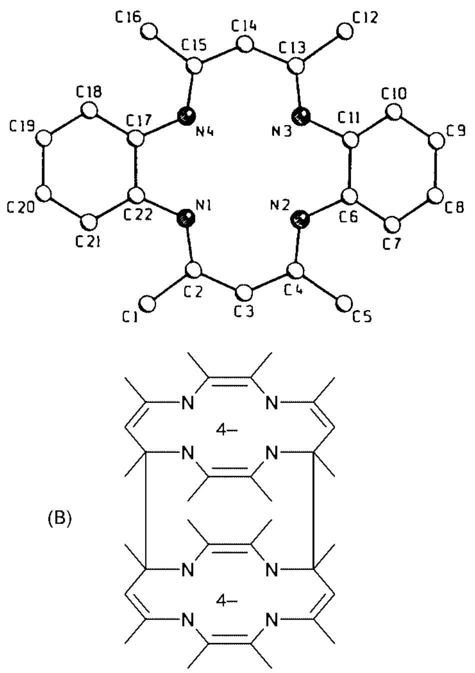

*tmtaa*₂

Chart 1 (A) The labeling scheme of the tmtaa anion. (B) The octa-anionic dinucleating ligand, *tmtaa*$_2$.

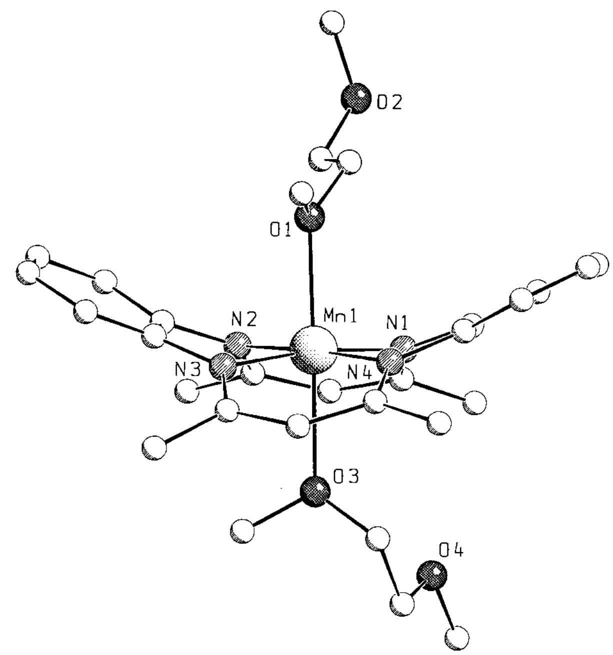

Fig. 2 A SCHAKAL view of the cation in complex **4b**.

dihedral angle of 1.9(1)° with the normal to the N_4 core. The Mn–N bond distances (mean value 1.930(7) Å) are slightly shorter than those observed in **3**. The saddle shape conformation of the tmtaa ligand does not differ remarkably from that observed in **3** (Table 3). The five-membered chelation rings are folded along the N···N lines (for dihedral angles see Table 3), manganese being displaced by 0.602(2) and 0.613(1) Å from the mean planes through the N(1),C(22),C(17),N(4) and N(2),C(6),C(11),N(3) atoms, respectively. The six-membered chelation rings are also folded along the N···N lines, the dihedral angles Mn,N(1),N(2) ∧ N(1),C(2),C(3),C(4),N(2) and Mn,N(3),N(4) ∧ N(3),C(13),C(14),C(15),N(4) being 24.2(2)° and 22.1(2)°, respectively. The binding ability of Mn(III) in the cationic form **4** suggests how to take advantage of both axial positions for making chain-like structures. In addition to the generation of cationic forms, complex **3** can be employed for a variety of functionalisations of Mn(III), including the formation of organometallic derivatives. A single example is reported in Scheme 1 with replacement of chloride by the isothiocyanate ligand. The characterisation of **5** (ν_{NCS} = 2053 cm^{-1}) is reported in the Experimental section, while the magnetic properties are analysed in section **B**.

The reaction of NO with transition metal ions[20] is of fundamental chemical and biological interest, namely for those metals, like manganese, which participate in redox reactions. Although rather rare, the formation of nitrosyl complexes of Mn(II) bonded to macrocyclic ligands is known.[21] The reaction of **1a** with NO led to the nitrosyl complex **6**, displaying some unusual magnetic properties, which have been analysed in detail (see next section) and are diagnostic for the electronic configuration and, eventually, the oxidation state of the metal. The ν_{NO} stretching vibration [1685 cm^{-1}] in **6** is in agreement with the presence of either Mn^{I}-$[NO]^{+}$ or Mn^{III}-$[NO]^{-}$. Although this is a formalism currently used in describing the {M–NO} functionality, we believe that the data we provide on **6** would lead to a different picture. The structural parameters derived from the X-ray analysis of **6** and the interpretation of the magnetic behaviour along with extended Hückel calculations were helpful for this purpose.

The structure of complex **6** is reported in Fig. 3. Manganese shows a slightly distorted square pyramidal coordination with the metal being displaced by 0.448(2) Å from the N_4 core, which shows tetrahedral distortions at the limit of significance (Table 3). The saddle shape conformation of the tmtaa ligand closely resembles that of complex **3** (see Table 3). The value of the metal out-of-plane displacement is rather close to what is expected for a d^6 configuration,[9] as is the linearity of the Mn–N–O functionality [174.9(6)°]. The Mn–N bond distances (Table 2) are rather close to those in the Mn(III) derivatives, **3** and **4b**, and much longer than those in the Mn(II) complex [Mn(tmtaa)·(NEt$_3$)] [Mn–N_{av} = 2.12 Å].[6] Although the Mn–N bond distances are in favor of a $Mn(III)^+$–NO^- formulation, such a conclusion cannot be drawn on this basis alone. A number of additional findings, for example the short Mn–N5 [1.612(8) Å], the rather long N5–O1 [1.208(11) Å] bond distances and the reaction of **6** with pyridine leading to a diamagnetic nitrosyl **7** [ν_{NO}, 1700 cm^{-1}], are much better accommodated using a cumulene Mn=N=O structure, than a pseudo-ionic formalism (see the following section). A useful comparison should be made with [Mn–NO] functionality supported by a macrocyclic environment[21] [Mn(NO)(TPP)], [Mn(NO)(TC-5,5)] and [Mn(NO)(BS)] (where TPP = 5,10,15,20-tetrakis-(phenyl)porphyrin, TC-5,5 = tropocoronand and BS = Schiff base = 2,12-di(2-pyridyl)-3,7,11-triazatrideca-2,11-diene).[22] The latter one, having quite remarkable short Mn–N and long N–O distances, fits very well with a cumulene-type picture.

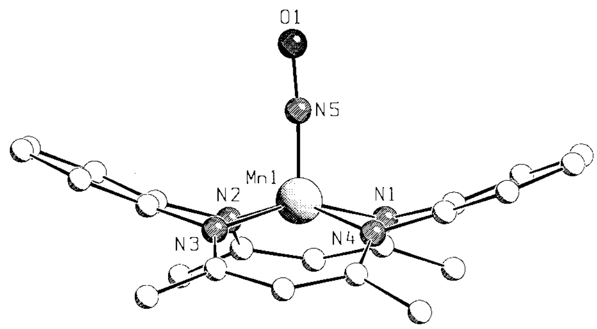

Fig. 3 A SCHAKAL view of complex **6**.

Attempts to generate oxo species out of the reaction of **1**, thus increasing, among others, the oxidation state of Mn up to (IV), have so far been unsuccessful, because we were unable to characterise any compound derived from the reaction with dioxygen. The redox chemistry associated with metal-macrocycles is particularly relevant, since both the metal and the ligand can be involved in the process either synergetically or independently of each other. Such synergism has very often been observed in metallaporphyrins.[23] In the case of Mn(II)-macrocycle complexes, due to the metal's reluctance to be reduced to lower oxidation states, reduction would affect mainly the ligand. This has been recently observed in the reduction of Mn(II)-Schiff base complexes.[24]

The reaction of **1a** with sodium metal was, however, more complex because of its dependence on the solvent used. When the reaction was run in DME (see Scheme 2), independent of the Mn/Na ratio, we observed the deprotonation of one of the methyl groups, forming a sodium organometallic intermediate **[C]**, collapsing to the dimeric complex **8**. Such bifunctional complexes have been recently produced in the reaction between [Mn(acacen)] [acacen = *N*,*N′*-ethylenebis(acetylacetone)iminato dianion] and lithium alkyls.[25] The metallate derivative **8** occurs in a dimeric ion pair form, with sodium cations remaining bound to the macrocyclic structure (Fig. 4). Manganese is in a square pyramidal environment. The metal is displaced by 0.832(2) Å from the mean plane through the N_4 core, which shows little, but non-trivial, tetrahedral distortion (Table 3). The Mn–C(1)′ vector (′ = $-x$, $-y$, $1-z$) forms a dihedral angle of 11.6(2)° with the normal to the N_4 mean plane. The Mn–N bond distances (mean value 2.109(7) Å) are longer than those reported for **3**, **4b**, and **6** (Table 2), as a

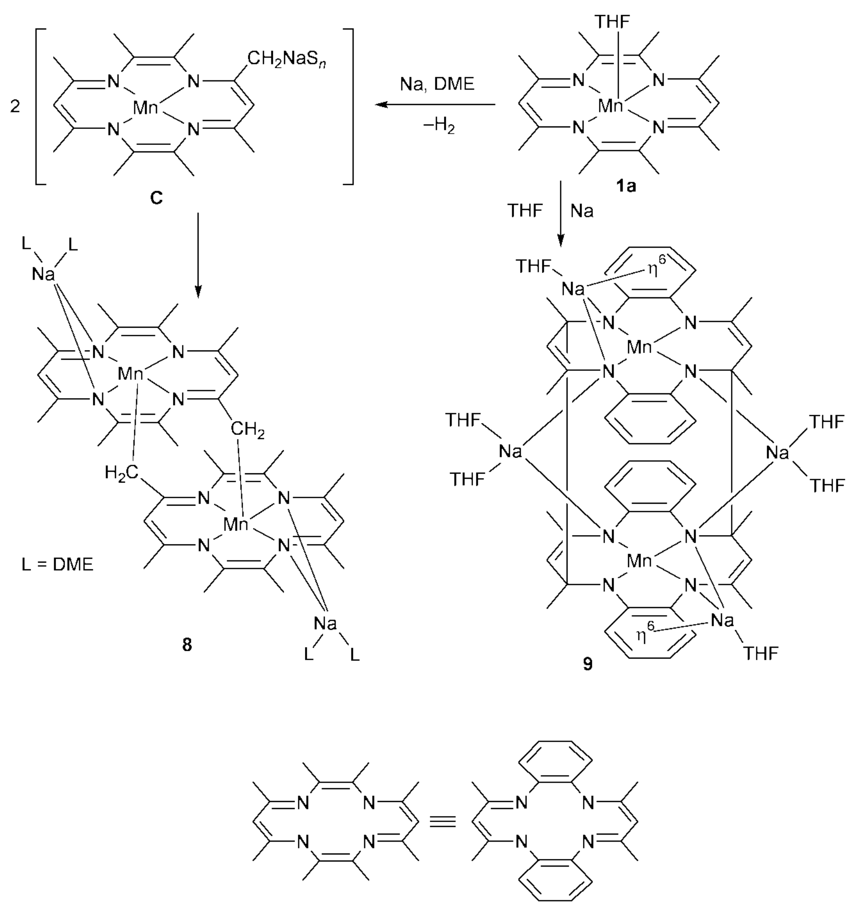

Scheme 2

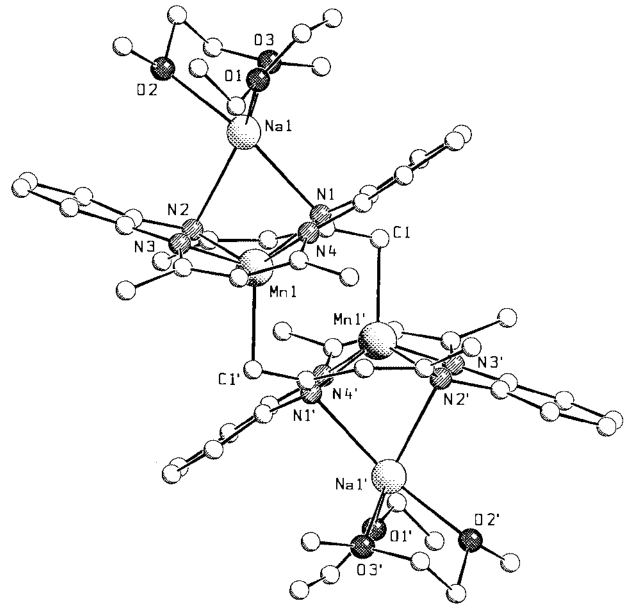

Fig. 4 A SCHAKAL view of complex **8**. Disorder affecting the solvent molecules bonded to Na(1) has been omitted for clarity. Primes denote a transformation of $-x$, $-y$, $1 - z$.

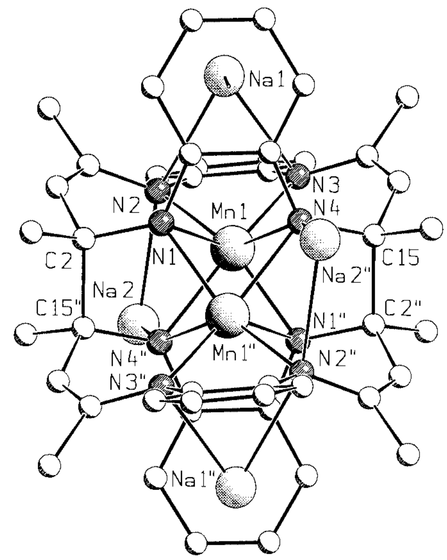

Fig. 5 A SCHAKAL view of molecule A in complex **9**. Disorder affecting the THF molecules bonded to Na(2) has been omitted for clarity. Primes denote a transformation of $-x$, $-y$, $-z$.

consequence of the remarkable out-of-plane distance and the electron richness of the metal. The Mn–C(1)′ bond distance falls in the lower range of values observed for Mn–C (primary alkyl) bond distances.[25] The N–C and C–C bond distances (Table 2) follow the usual trend. The saddle shape conformation of the tmtaa ligand is not remarkably affected by the bridging role of the C(1) carbon atom (Table 3). The five-membered chelation rings are nearly planar (dihedral angles: Mn,N(1),N(4) $\wedge$ N(1),C(22),C(17),N(4), 9.7(2)°; Mn,N(2),N(3) $\wedge$ N(2),C(6),C(11),N(3), 9.9(3)°), manganese being displaced by 0.278(1) and 0.283(1) Å from the mean planes through the N(1),C(22),C(17),N(4) and N(2),C(6),C(11),N(3) atoms, respectively. The six-membered chelation rings are remarkably folded along the N···N lines, the dihedral angles Mn,N(1),N(2) $\wedge$ N(1),C(2),C(3),C(4),N(2) and Mn,N(3),N(4) $\wedge$ N(3),C(13),C(14),C(15),N(4) being 51.4(2)° and 50.4(2)°, respectively. The sodium cation interacts with the N(1) and N(2) nitrogen atoms at rather long distances (Na–N(1), 2.520(6); Na–N(2), 2.542(6) Å).

When the reaction between Na metal and **1a** was carried out in THF, the Mn/Na molar ratio became crucial, thus the formation of **8** was still observed with one equivalent of Na per Mn. With a Mn/Na = 1 : 2 molar ratio, the reduction of [Mn(tmtaa)] led instead to the formation of **9**.

Complex **9** derives from a double reductive coupling of two imino groups across two [Mn(tmtaa)] units. This reductive coupling is known to occur when a metal, which is reluctant to be reduced, is bonded to a polydentate Schiff base ligand, such as salophen [salophen = *N*,*N*′-phenylenebis(salicylidene)-iminato dianion].[24,26] Such a coupling reaction transformed the two tmtaa moieties into a dimeric octaanionic dinucleating ligand (Chart 1B), without any change in the oxidation state of the metal. The rather complex structure of **9** has been clarified by X-ray analysis.

The structure of **9** consists of the packing of two independent dimeric complex molecules (called molecule A and B) (Fig. 5). The dimers being of very similar structure and geometry, discussion will be restricted to molecule A. Values referring to molecule B will be given in square brackets. The dimers originate from the formation of two C–C bonds occurring between the C(2) and C(15) imino carbon atoms from a Mn(tmtaa) moiety and the C(15)″ and C(2)″ atoms from a centrosymmetric one. As a result each independent manganese atom achieves hexa-coordination through the nitrogen atoms from a N_4 core and the N(1)″ and N(4)″ nitrogen atoms from the symmetrically related tmtaa ligand. The coordination polyhedron could be described as a trigonal prism with the N(1), N(2), N(4)″ and N(3), N(4), N(1)″ atoms defining the bases, the dihedral angle between then being 0.7(2) [0.6(2)]°. The metal is displaced by 1.356(1) [1.235(2)] and 1.227 [1.348] Å from the N(1), N(2), N(4)″ and N(3), N(4), N(1)″ planes, respectively. In the dimer the two trigonal prisms share the N(1), N(4), N(1)″ N(4)″ face. The N_4 core shows little, but significant, tetrahedral distortion (Table 3), the metal being displaced by 0.868(2) [0.864(1)] Å from it. The Mn–N bond distances fall in a rather wide range (Table 2), in particular the Mn–N(1) (2.274(5) [2.336(5)] Å) and the Mn–N(4) (2.319(5) [2.257(5)] Å) bond distances bridging the two manganese metals are remarkably longer than the others, as expected. The trend of the N–C and C–C bond distances and angles within the tetraanionic tmtaa ligand is consistent with a double bond character of the C(3)–C(4) (1.349(9) [1.336(10)] Å) and C(13)–C(14) (1.353(10) [1.351(9)] Å) bonds. The values of the C(2)–C(15)″ bond distances (1.699(8) [1.671(9)] Å) are consistent with those generally observed for bond distances involving the imino carbon atoms of adjacent tmtaa ligands. The presence of interligand C–C bonds strongly affects the conformation of the macrocycle, in particular the two NC_6N systems are oriented to be nearly perpendicular, as indicated by the dihedral angle of 92.4(1) [92.2(1)]° formed by the NC_6N mean planes (Table 3). In addition, the NC_3N systems turn out to be nearly coplanar with the N_4 core ($N_4 \wedge N(1)C_3N(2)$, 168.2(2) [172.8(1)]°; $N_4 \wedge N(3)C_3N(4)$, 172.5(2) [169.1(2)]°). This conformation provides suitable room for anchoring two sodium cations, the Na(1) cation interacting with the N(2), N(3) nitrogen atoms and the Na(2) cation with the N(2), N(4)″ [N(3), N(4)″ in molecule B] atoms. Coordination around Na(1) is completed through interaction with the O(1) oxygen atom from a THF molecule and through η^6-interaction with the C(17)···C(22) aromatic ring. The η^6-bonding mode is supported by the narrow range of the Na(1)···C interactions (2.744(8)–2.868(7) Å [2.714(7)–2.830(7) Å]). Coordination around Na(2) is completed by interaction with the O(2) and O(3) oxygen atoms from two THF molecules.

The two tetraanionic compartments of the ligand in Chart 1B sharing the four nitrogen donor atoms force the two Mn ions into a close geometrical proximity [Mn···Mn, 2.569(2) and 2.563(2) Å for molecule A and B respectively]. The rather intriguing magnetic and electronic properties due to the dimeric nature of **9** and the close proximity of the two Mn(II) are

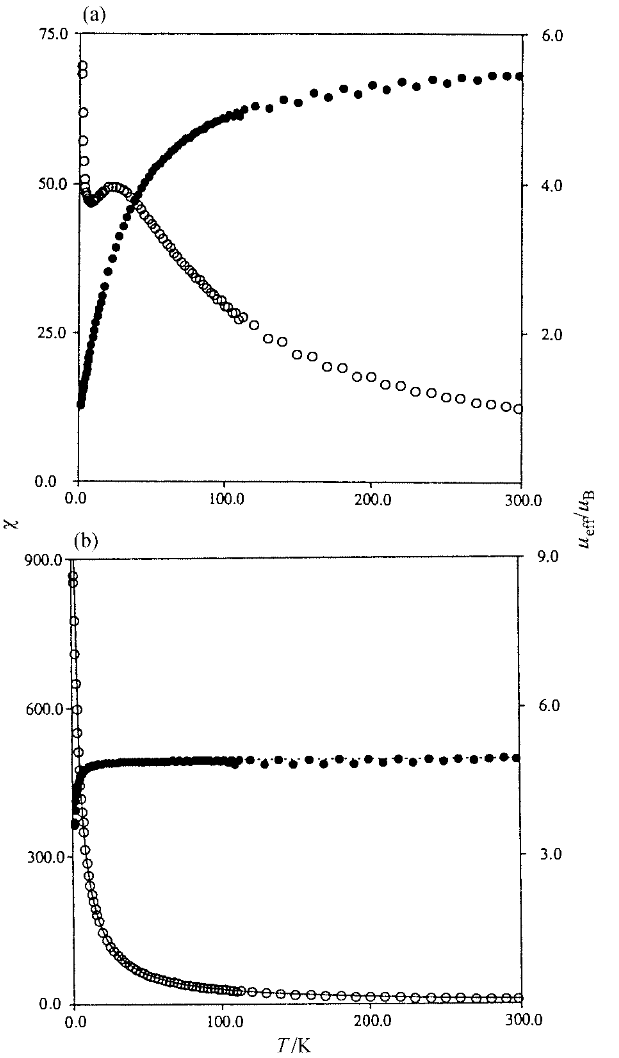

Fig. 6 Magnetic susceptibilities (○) and magnetic moments (●) as a function of the temperature (a) for complex **1b**; (b) for complex **3**.

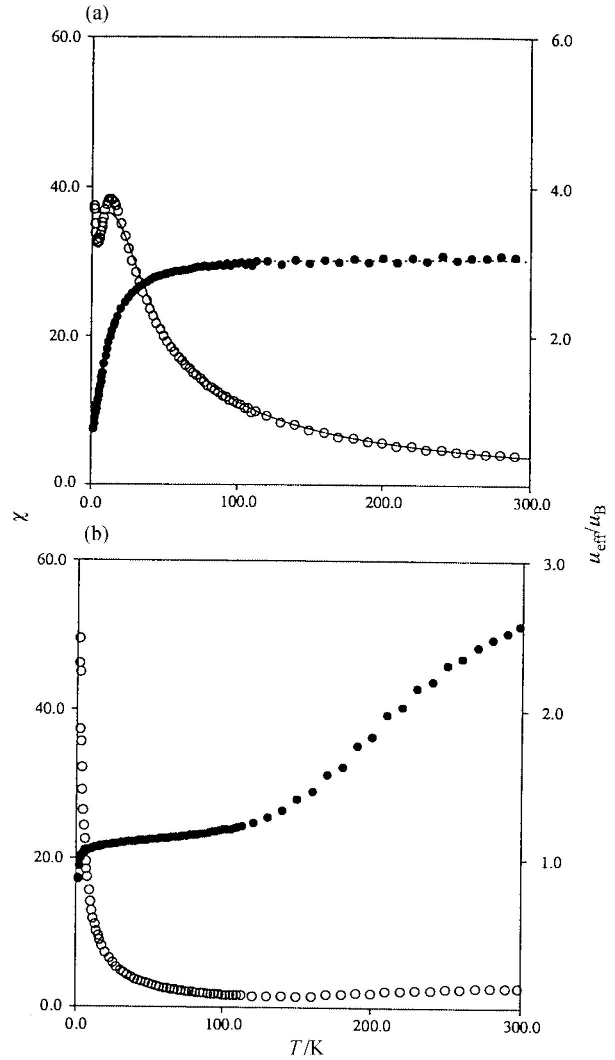

Fig. 7 Magnetic susceptibilities (○) and magnetic moments (●) as a function of the temperature (a) for complex **4b**; (b) for complex **6**.

analysed in the next section. The property associated to the C–C bonds present in the structure of **9** and derived from a reductive coupling has to be emphasised, namely in the case of manganese which has a relevant redox chemistry. The C–C bonds mentioned above usually function as shuttles for two electrons, thus they cleave when the metal complex reacts with a variety of oxidising agents.[24,26]

B Magnetic Properties

The magnetic susceptibilities (in units of 10^{-3} cm^3 mol^{-1}) of complexes **1**–**9** were measured in the temperature range 1.9–300 K and those of **1b**, **3**, **4b**, **6**, **8**, and **9** are shown in Fig. 6, 7 and 8.

The temperature dependence of the magnetic moments of **1a** is typical of a high spin Mn(II) d^5 monomer ($S = 5/2$), the magnetic moment being constant in almost the entire temperature range 2–300 K with a value of 5.85 μ_B. A different behavior is observed for **1b** whose magnetic moment has a value of 5.40 μ_B at 298 K which remains almost constant between 300 and 100 K and then decreases suddenly, reaching a value of 1.00 μ_B at 2.0 K (see Fig. 6a). This behavior is compatible with a $S = 3/2$ intermediate spin state, assuming that the high value of the magnetic moment at room temperature (5.40 μ_B much larger than the spin-only value of 3.88 μ_B) is due to the admixing of the low lying $S = 5/2$ state into the ground state wavefunction. It is worth noting that the analogous tetracoordinated manganese(II) phthalocyanine has a $S = 5/2$ ground state with a large value of the magnetic moment at room temperature (*ca.* 4.4 μ_B).[27]

The temperature dependence of the magnetic moments of **3** (Fig. 6b), **4c** and **5** is typical of high spin Mn(III) d^4 monomeric species, the magnetic moment is constant between 300 and 30 K and then shows a slight decrease due to zero-field splitting. This behavior can easily be fitted with an axial spin hamiltonian $H = \beta gH{\cdot}S + D[S_z^2 - S(S+1)/3]$,[28] where $S = 2$, g is the isotropic g-factor, D is the zero field splitting constant, and the calculated best fit parameters are reported in Table 4. Note that the calculated zero-field-splitting constants are relatively high, but in the range of the values calculated for analogous high-spin Mn(III)-porphyrin complexes.[29]

The temperature dependence of the magnetic moments of **4b** (Fig. 7a) indicates low spin Mn(III) d^4 monomeric species. The magnetic moment is nearly constant between 300 and 60 K, with a value of *ca.* 3.10 μ_B, and then decreases more sharply than for **3**, **4c** or **5**. The magnetic data have been fitted again with the spin hamiltonian[28] with $S = 1$ (see Table 4), although a satisfying fit has required the introduction of a temperature independent paramagnetism (TIP) term *Nα*.

A summary of the magnetic properties of polycrystalline samples of all the characterised [Mn(tmtaa)(L)(L′)] complexes is given in Table 4. We see that although most of these compounds are high-spin states (**3**, **4c**, **5**), one, **4b**, has a low-spin ground state. Low-spin manganese(III) compounds are very rare and only very few have been reported.[30] In particular, all of the d^4 manganese(III) porphyrin complexes have a high-spin state, the only exception being a imidazolate polymeric complex whose magnetic behavior has been interpreted in terms of alternate low-spin and high-spin manganese(III) centres.[31] In

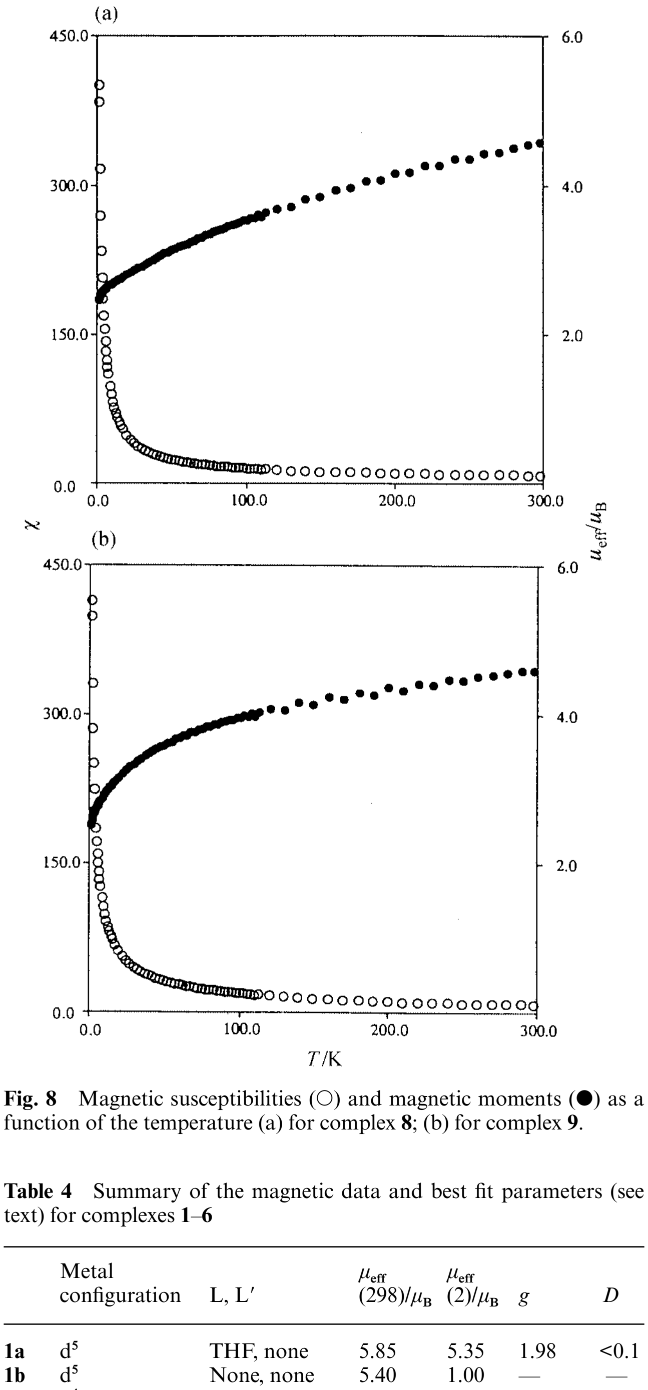

Fig. 8 Magnetic susceptibilities (○) and magnetic moments (●) as a function of the temperature (a) for complex **8**; (b) for complex **9**.

Table 4 Summary of the magnetic data and best fit parameters (see text) for complexes **1**–**6**

	Metal configuration	L, L′	μ_{eff} (298)/μ_B	μ_{eff} (2)/μ_B	g	D
1a	d^5	THF, none	5.85	5.35	1.98	<0.1
1b	d^5	None, none	5.40	1.00	—	—
3	d^4	Cl, none	4.95	3.60	2.02	5.0
4b	d^4	DME, DME	3.10	0.70	2.14	43.0
4c	d^4	Py, none	4.85	3.20	1.96	6.9
5	d^4	SNC, none	4.90	3.20	1.98	6.8
6	$\{MnNO\}^6$	NO, none	2.55	0.80	—	—

spite of the few available complexes, it is possible to infer some trends on the dependence of the spin state of the manganese(III) centre on the nature and the number of axial ligands. Weak-field ligands and coordination numbers less than six favour high spin systems.

The temperature dependence of the magnetic moment of the nitrosyl complex **6** shows the occurrence of a spin-transition above 80 K (Fig. 7b). Three spin states are possible for this $\{MnNO\}^6$ species, *i.e.* $S = 0, 1, 2$. The low-temperature value of the moment (*ca.* 0.9 μ_B) is not zero as expected for the diamagnetic low-spin state ($S = 0$), indicating the presence of a residual amount of higher spin species. Raising the temperature above 80 K results in an increase of the magnetic moment reaching a value of 2.55 μ_B at 298 K that is compatible with either

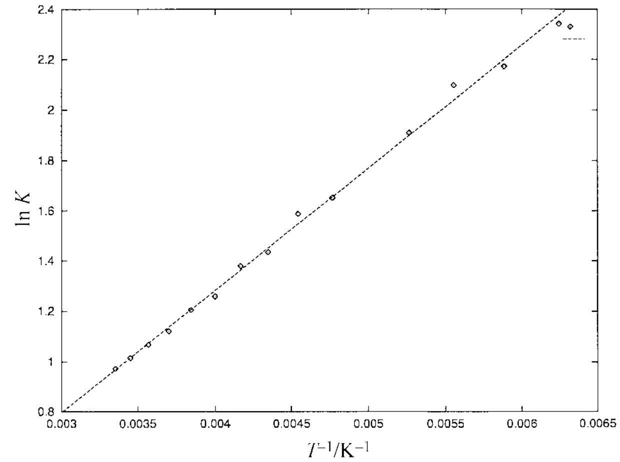

Fig. 9 Plot of ln K *vs.* $1/T$ for the LS–HS spin equilibrium in complex **6**.

an intermediate-spin ($S = 1$) or a high-spin ($S = 2$) state. The spin-transition occurs rather smoothly, suggesting weak intermolecular interactions within the crystal lattice, and is still not complete at the highest measured temperature of 300 K.

To distinguish between the two possible high-spin states involved in the spin equilibrium, *i.e.* $S = 1$ *vs.* $S = 2$, we fitted the magnetic data to a thermodynamic model. The high-spin mol fraction n_{HS} was calculated at every temperature according to the relation: $n_{HS} = \dfrac{\chi_M T - (\chi_M T)_{LS}}{(\chi_M T)_{HS} - (\chi_M T)_{LS}}$, where $(\chi_M T)_{LS} = 0$ and $(\chi_M T)_{HS} = N\mu_B^2 g^2 S(S+1)/k$, with $S = 1$ or 2, and $g = 2.0$ or 2.2, respectively. Depending on the choice of the high-spin state, the percentage of the high-spin species was found to be *ca.* 68% or 27% at 298 K, while the residual amount of high-spin at 2 K was 8% or 3%, respectively for $S = 1$ or $S = 2$. A plot of ln K as a function of T^{-1}, K being the formal constant of the equilibrium LS ↔ HS defined as $K = n_{HS}/(1 - n_{HS})$, has been generated for both $S = 1$ and $S = 2$ choices. A linear plot has been obtained only for $S = 2$ in the range 170–300 K (Fig. 9), thus a $S = 0 \leftrightarrow S = 2$ spin equilibrium. This result also allows one to estimate the energy gap between the fundamental low-spin singlet and the high-spin triplet state by using the relation $-\ln K = \Delta H_{eff}/RT - \Delta S_{eff}/R$, where ΔH_{eff} and ΔS_{eff} are the effective enthalpy and entropy changes associated with the spin-transition within a finite domain model.[32] A best fit of the data between 170 and 300 K allowed evaluation of the two parameters as $\Delta H_{eff} = 4.0$ kJ mol^{-1} and $\Delta S_{eff} = 11.3$ J mol^{-1} K^{-1}. Note that the evaluated ΔS_{eff} value is very close to the spin only value $\Delta S_{spin} = R\ln[(2S + 1)_{HS} - (2S + 1)_{LS}] = 11.5$ J mol^{-1} K^{-1}, thus confirming that, within a domain model,[32] the transition shows negligible cooperative effects. The magnetic behavior of **6** is quite peculiar compared to the diamagnetism of other manganese nitrosyls based on N_4 or N_3O_2 ligands.[21,33] The only exception is the recently characterised [Mn(NO)(TC-5,5)] complex which shows a high-spin $S = 2$ state.[21c] The coordination of a pyridine to the nitrosyl complex stabilises the low-spin state $S = 0$, as proved by the diamagnetism of compound **7**.

The magnetic behavior of the two Mn(II) dimers **8** and **9** is quite peculiar and difficult to interpret unambiguously. The magnetic moment of **8** shows a value of 4.45 μ_B at 298 K and decreases steadily reaching 2.40 μ_B at 2 K (Fig. 8a). Taking into account that a negligible magnetic interaction is expected through the triatomic –CH_2–C–N– bridge, such a behavior can be attributed to either a spin-crossover or a spin admixing involving a low-spin, $S = 1/2$, and a $S = 3/2$ or $S = 5/2$ state on each Mn(II) centre. The ESR spectrum of a frozen THF solution at 110 K shows an "axial" pattern with $g_{\parallel} = 2.1$ and a $g_{\perp} = 5.2$. The $g_{\perp}$ value is intermediate between the values of 4.0 and 6.0 expected for pure $S = 3/2$ and $S = 5/2$ states and

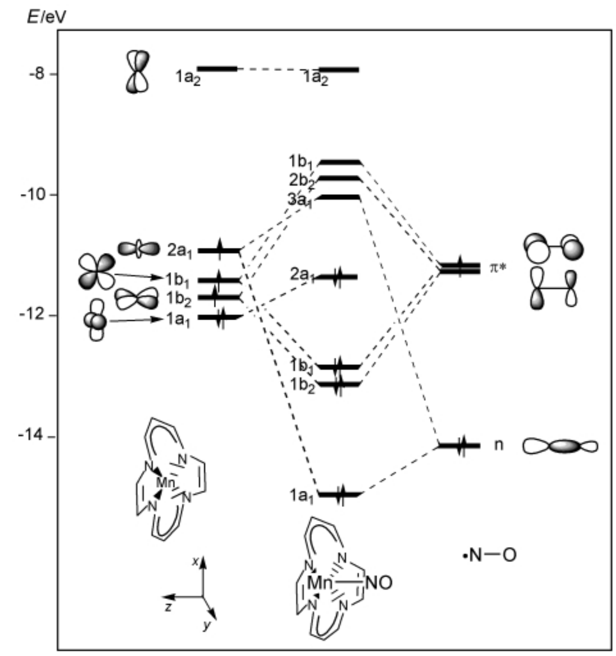

Fig. 10 Orbital interaction diagram for complex **6**.

thus supports the presence of a spin-admixed 3/2–5/2 state. Low-spin manganese(II) complexes are quite rare,[34] but a $S = 1/2$ ground state is not completely unexpected for such a square-pyramidal coordination with a strong equatorial field from the tetradentate macrocyclic ligand.

The magnetic moment of **9** has a value of 4.50 μ_B at 298 K and decreases first slightly and then more sharply reaching 2.55 μ_B at 2 K (Fig. 8b). This behavior is compatible with an isolated quintet ground state ($S = 2$) for the strongly coupled metal–metal bonded Mn_2 dimer while the decrease at low temperature is attributed to zero-field splitting. Such an interpretation has been supported by extended Hückel calculations, see below.

C Extended Hückel analysis

Extended Hückel (EH) calculations[35] were performed to gain a better understanding of the significant magnetic properties of the manganese(III) complexes supported by the tmtaa ligand and the electronic structure of the nitrosyl complex **6**. The tmtaa ligand has been simplified by replacing the benzene units by ethylene and the methyl groups by hydrogens. Such a simplified model has already been employed in EH[36] and SCF-Xα-SW (self-consistent field-Xα-standing waves)[37] calculations and showed a good correlation with the results obtained with the whole ligand.[37] The molecular orbitals of the [Mn(tmtaa)] fragment are reported on the left of Fig. 10. The metal orbitals mix strongly with the ligand frontier orbitals so that no pure d orbitals can be assigned. However, five molecular orbitals with large metal d character can be identified. These are the doubly occupied orbitals $1a_1(d_{x^2-y^2})$, and the three singly occupied $1b_2(d_{yz})$, $1b_1(d_{xz})$, and $2a_1(d_{z^2})$. The $1a_2(d_{xy})$ pointing more closely towards the nitrogen atoms of tmtaa, is pushed to higher energy.

The interaction between the [Mn(tmtaa)] fragment and the NO unit is illustrated by the molecular orbital diagram for the [Mn(tmtaa)(NO)] complex, **6**, in Fig. 10. The molecular orbitals of the [Mn(tmtaa)] described above are reported on the left while on the right we report the frontier orbitals of NO, *i.e.* the σ-donor lone pair on N, n, and the doubly degenerate π*(NO) orbitals occupied by the unpaired electron. Fig. 10 shows a strong interaction between the $2a_1(d_{z^2})$ and the σ-donor n of NO and between the two dπ metal orbitals, $1b_1(d_{xz})$ and $1b_2(d_{yz})$, and the degenerate π* orbitals of NO, which are typical of metal nitrosyl species.[38] The non occupancy of the $3a_1(d_{z^2}\sigma)$ antibonding orbital of the nitrosyl complex (which would be stabilised by the mixing with one of the π* upon bending) favors a linear MnNO angle in agreement with the observed X-ray structure of **6** which is consistent with other analogous structurally characterised $\{MnNO\}^6$ compounds.[21] Note from Fig. 10 that the two d_π orbitals of the Mn(tmtaa) fragment, b_1 and b_2, are very close in energy to the two π* orbitals of NO so that the molecular orbital of the nitrosyl complex resulting from their interaction has a strong π*(NO) character.

This has important consequences for the properties of the nitrosyl complex **6**. The bond formation between manganese and NO cannot be described in terms of a donation from the π*(NO) to the metal which would lead to Mn(I) and NO^+ as usually accepted for a linear M–NO unit. Instead, a strong back-donation to NO is forecast which would rather suggest a formal oxidation state of Mn(III) for the metal, in agreement with the observed Mn–N bond distances which are shorter than those in Mn^{II}(tmtaa) (see above). Moreover, the significant population of the π*(NO) antibonding orbitals (1.8 e) leads to a strong reduction of the N–O bond order and an increase of the Mn–N bond order and suggests a Mn=N=O valence structure, in agreement with the observed structural parameters for the Mn–NO unit (see above).

The magnetic behavior of the nitrosyl complexes **6** and **7** can be understood on the basis of the extended Hückel molecular orbital scheme for **6** in Fig. 10. The low-spin ground state of this $\{MnNO\}^6$ species corresponds to the double occupancy of the three lowest $1b_1(d_{xz}-\pi^*)$, $1b_2(d_{yz}-\pi^*)$ and $2a_1(d_{x^2-y^2})$ predominantly metal orbitals, while the low-lying quintet state arises from a two-electron excitation to the higher $3a_1(d_{z^2})$. The *trans*-coordination to a strong σ-donor ligand raises the $3a_1(d_{z^2})$ and $1a_2(d_{xy})$ orbitals (the latter through a decrease of the metal out-of-plane distance) thus destabilising the quintet state and is therefore expected to lead to a diamagnetic species, as actually observed for the pyridine adduct **7**.

An extended Hückel analysis probably allows one to better understand why the reduction of **1a** occurs at the ligand, to give a picture of the electronic configuration of **9**, and the explanation of its magnetic properties.

The lowest unoccupied orbital of [Mn(tmtaa)] is the $8a_2$ which is essentially the lowest π* orbital of the $(tmtaa)^{2-}$ ligand slightly mixed with the metal d_{xz} as is illustrated in Chart 2A.

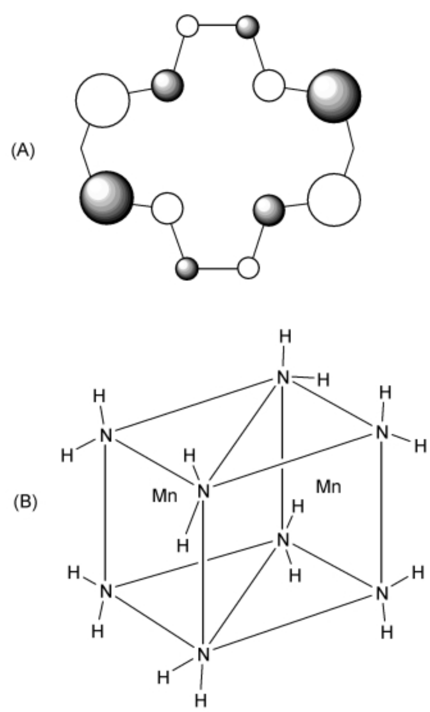

Chart 2 (A) Lowest unoccupied molecular orbital, $8a_2$, of [Mn(tmtaa)]. (B) Octaamido model of the prismatic skeleton of **9**.

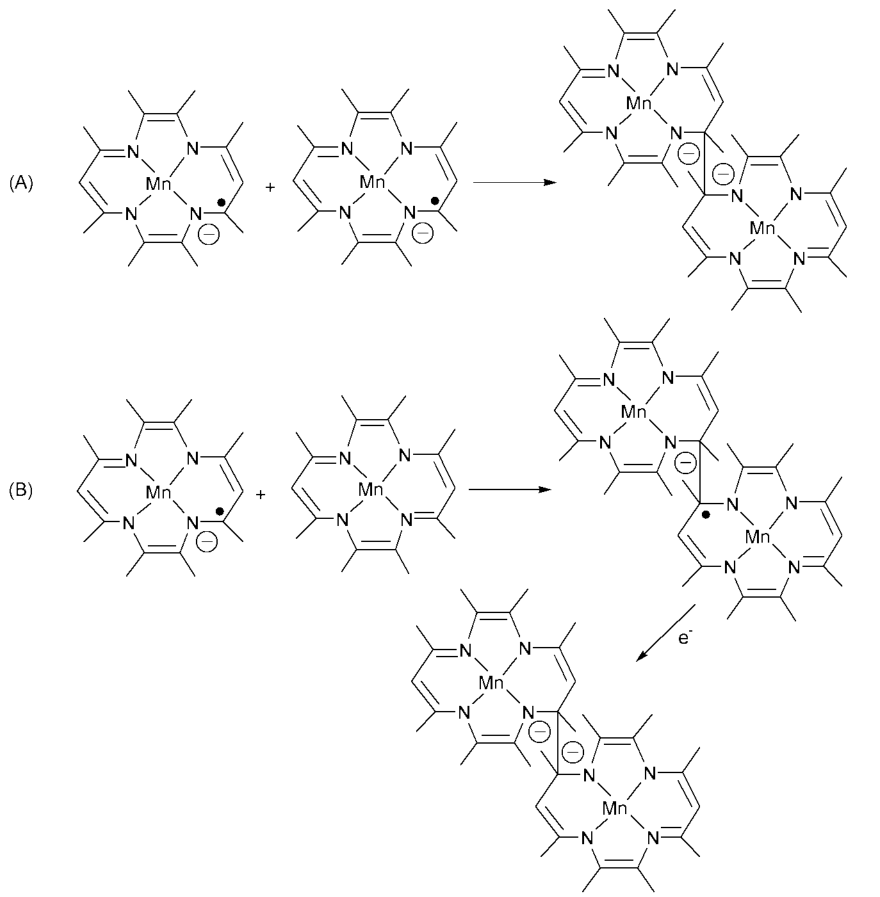

Scheme 3 Proposed mechanism for the C–C dimerisation of tmtaa.

This orbital is mainly localised on the imino carbons so that the resulting $[Mn(tmtaa)]^-$ anion is expected to have a marked radical character localised on these carbon atoms. The C–C bond formation is then reached either by dimerisation of two radical anions or by the addition of one radical anion to a neutral species leading to a dimeric radical, which is subsequently reduced to the final dimer **9** (pathways **A** and **B** in Scheme 3). The preliminary stage of the reaction of **1a** with sodium metal may be the formation of the same radical anion precursor leading to **8**, *via* the deprotonation of one of the methyl groups, or dimerising to **9**. Which pathway is selected is strongly dependent on the reaction solvent, which affects both the reduction and the deprotonation properties of Na, and the sterically controlled dimerisation of the intermediate ion-pair [Mn(tmtaa)Na] form.

Extended Hückel calculations have been performed on a simplified model of **9** in which the octaanionic $^*tmtaa_2{}^*$ ligand has been replaced by eight NH_2^- groups with the Mn–N distances and H–N–H angles taken from the Mn–N distances and C–N–C angles in the real complex. Such an octaamido model retains the prismatic skeleton of the Mn_2N_8 core of **9** (see Chart 2B) and is expected to preserve the same metal orbital pattern. Analogous tetraamido simplified models have already been employed in EH calculations on N_4 macrocyclic complexes such as porphyrins and the resulting metal orbital patterns correlated very well with those obtained with the whole ligand.[36a,39] The molecular orbital diagram of $[Mn_2(NH_2)_8]^{4-}$ in D_{2h} symmetry has been built from the $[Mn(NH_2)_2]_2$ and $(NH_2)_4{}^{4-}$ fragments and is reported in Fig. 11. The four lowest levels of $[Mn(NH_2)_2]_2$ correspond to the bonding combinations of the metal d_{z^2}, $d_{x^2-y^2}$, d_{yz} and d_{xy} orbitals (see sketches in Fig. 11), while the next four levels are the corresponding antibonding combinations. The d_{xz} orbitals pointing toward the amido ligands are strongly destabilised and their bonding and antibonding combinations are the highest in energy. Due to a favorable interaction with the orbitals of proper symmetry of the bridging four amido groups, some of the above orbitals are destabilised, particularly the three bonding combinations $b_{2u}(\pi_{yz})$, $b_{1g}(\delta_{xy})$ and $b_{3u}(\pi_{xz})$, see Fig. 11. The almost degeneracy of the four b_{3g} b_{2u} a_u and b_{1u} levels suggests a quintet ground state in agreement with our interpretation of the magnetic behavior. The resulting $(\sigma)^2(\delta_{x^2-y^2})^2(\delta^*_{xy})^2(\pi^*_{yz})^1$-

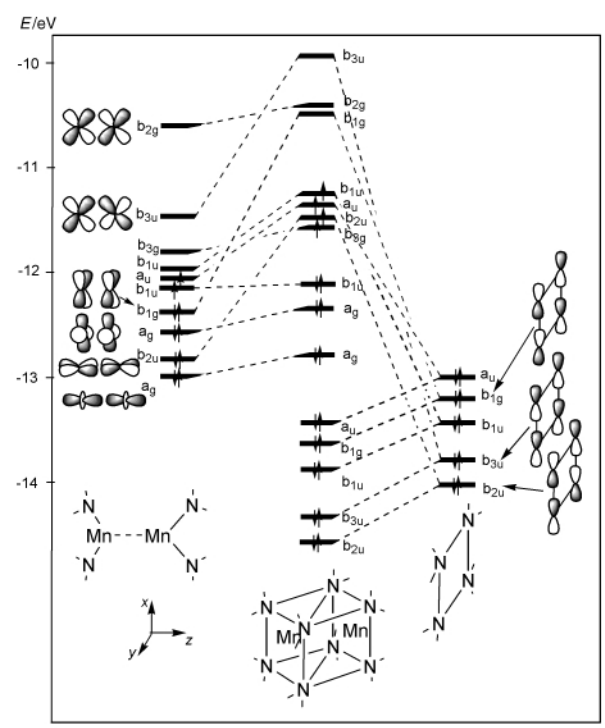

Fig. 11 Orbital interaction diagram for $[Mn_2(NH_2)_8]^{4-}$.

$(\pi_{yz})^1(\delta^*_{x^2-y^2})^1(\sigma^*)^1$ configuration indicates little metal–metal bond character, mainly as a consequence of the destabilisation of the three bonding π_{yz}, δ_{xy} and π_{xz} orbitals by the four bridging NH_2^- ligands. This is as also evidenced by the small Mn–Mn overlap (0.17), which is smaller than that calculated for the unbridged $[Mn(NH_2)_2]_2$ fragment.

Acknowledgements

We thank the "Fonds National Suisse de la Recherche Scientifique" (Bern, Switzerland, Grant No. 20-53336.98), Fondation Herbette (University of Lausanne, N. Re), and Action COST D9 (European Program for Scientific Research, OFES No. C98.008) for financial support.

References

1 (*a*) *Photosynthesis*, ed. W. R. Briggs, ARL, New York, 1989; (*b*) K. Wieghardt, *Angew. Chem., Int. Ed. Engl.*, 1989, **28**, 1153; (*c*) G. W. Brudwig and R. H. Crabtree, *Prog. Inorg. Chem.*, 1989, **37**, 99; (*d*) *Manganese Redox Enzymes*, ed. V. L. Pecoraro, VCH, New York, 1992; (*e*) *The Photosynthetic Reaction Center*, eds. J. Deisenhofer and J. R. Norris, Academic Press, New York, 1993, vol. I and II; (*f*) G. C. Dismukes, *Chem. Rev.*, 1996, **96**, 2909.

2 V. L. Pecoraro, M. J. Baldwin and A. Gelasco, *Chem. Rev.*, 1994, **94**, 807.

3 M. K. Stern and J. T. Groves, in *Manganese Redox Enzymes*, ed. V. L. Pecoraro, VCH, New York, 1992, ch. 11.

4 (*a*) E. N. Jacobsen, in *Comprehensive Organometallic Chemistry II: a Review of the Literature 1982–1994*, eds. E. W. Abel, F. G. A. Stone and G. Wilkinson, Pergamon, Oxford, 1995, vol. 12, ch. 11.1; (*b*) S. I. Murahashi and T. Naota, in *Comprehensive Organometallic Chemistry II: a Review of the Literature 1982–1994*, eds. E. W. Abel, F. G. A. Stone and G. Wilkinson, Pergamon, Oxford, 1995, vol. 12, ch. 11.3.

5 (*a*) E. N. Jacobsen, W. Zhang, A. R. Muci, J. R. Ecker and L. Deng, *J. Am. Chem. Soc.*, 1981, **113**, 7063; (*b*) P. J. Pospisil, D. H. Carsten and E. N. Jacobsen, *Chem. Eur. J.*, 1996, **2**, 974.

6 M. C. Weiss, B. Burstein, S. M. Peng and V. L. Goedken, *J. Am. Chem. Soc.*, 1976, **98**, 8021.

7 E. Solari, F. Musso, E. Gallo, C. Floriani, N. Re, A. Chiesi-Villa and C. Rizzoli, *Organometallics*, 1995, **14**, 2265.

8 V. L. Goedken and M. C. Weiss, *Inorg. Synth.*, 1980, **20**, 115.

9 S. De Angelis, E. Solari, E. Gallo, C. Floriani, A. Chiesi-Villa and C. Rizzoli, *Inorg. Chem.*, 1992, **31**, 2520.

10 E. A. Boudreaux and L. N. Mulay, *Theory and Applications of Molecular Paramagnetism*, Wiley, New York, 1976, pp. 491–495.

11 The anhydrous salt was prepared according to a published procedure: L. E. Manzer, *Inorg. Synth.*, 1982, **21**, 135.

12 TEXSAN for Windows: Crystal Structure Analysis Package, Molecular Structure Corporation, Houston, TX, 1997.

13 Z. Otwinowski and W. Minor, *Methods in Enzymology*, *Vol. 276*: *Macromolecular Crystallography*, *part A*, eds. C. W. Carter, Jr and R. M. Sweet, Academic Press, New York, 1997, pp. 307–326.

14 A. C. T. North, D. C. Phillips and F. S. Mathews, *Acta Crystallogr., Sect. A*, 1968, **24**, 351.

15 *International Tables for X-ray Crystallography*, Kynoch Press, Birmingham, 1974, vol. IV, (*a*) p. 99; (*b*) p. 149.

16 R. F. Stewart, E. R. Davidson and W. T. Simpson, *J. Chem. Phys.*, 1965, **42**, 3175.

17 G. M. Sheldrick, SHELX76, Program for crystal structure determination, University of Cambridge, 1976.

18 G. M. Sheldrick, SHELXL93, Program for crystal structure refinement, University of Göttingen, 1993.

19 (*a*) F. A. Cotton and J. Czuchajowska, *Polyhedron*, 1990, **9**, 2553; (*b*) P. Mountford, *Chem. Soc. Rev.*, 1998, **27**, 105.

20 G. B. Richter-Addo and P. Legzdins, *Metal Nitrosyls*, Oxford University Press, New York, 1992.

21 (*a*) W. R. Scheidt, K. Hatano, G. A. Rupprecht and P. L. Piciulo, *Inorg. Chem.*, 1979, **18**, 292; (*b*) D. J. Cooper, M. D. Ravenscroft, D. A. Stotter and J. Trotter, *J. Chem. Res.* (*M*), 1979, 3359; (*c*) K. J. Franz and S. J. Lippard, *J. Am. Chem. Soc.*, 1998, **120**, 9034.

22 In [Mn(NO)(TPP)]: Mn–N: 1.641 Å; N–O: 1.16 Å. In [Mn(NO)(TC-5,5)]: Mn–N: 1.699 Å; N–O: 1.179 Å. In [Mn(NO)(BS)]: Mn–N: 1.58 Å; N–O: 1.215 Å.

23 (*a*) *Porphyrins and Metalloporphyrins*, ed. K. M. Smith, Elsevier, Amsterdam, 1975; (*b*) *The Porphyrins*, ed. D. Dolphin, Academic Press, New York, 1978.

24 E. Gallo, E. Solari, N. Re, C. Floriani, A. Chiesi-Villa and C. Rizzoli, *J. Am. Chem. Soc.*, 1997, **119**, 5144.

25 (*a*) E. Gallo, E. Solari, C. Floriani, A. Chiesi-Villa and C. Rizzoli, *Organometallics*, 1995, **14**, 2156; (*b*) E. Gallo, E. Solari, C. Floriani, A. Chiesi-Villa and C. Rizzoli, *Inorg. Chem.*, 1997, **36**, 2178.

26 (*a*) S. Gambarotta, F. Urso, C. Floriani, A. Chiesi-Villa and C. Guastini, *Inorg. Chem.*, 1983, **22**, 3966; (*b*) S. De Angelis, E. Solari, E. Gallo, C. Floriani, A. Chiesi-Villa and C. Rizzoli, *Inorg. Chem.*, 1996, **35**, 5995; (*c*) E. Solari, C. Maltese, F. Franceschi, C. Floriani, A. Chiesi-Villa and C. Rizzoli, *J. Chem. Soc., Dalton Trans.*, 1997, 2903; (*d*) F. Franceschi, E. Solari, C. Floriani, A. Chiesi-Villa, C. Rizzoli and M. Rosi, *Chem. Eur. J.*, 1999, **5**, 708; (*e*) M. Rosi, A. Sgamellotti, F. Franceschi and C. Floriani, *Chem. Eur. J.*, 1999, **5**, 2914.

27 (*a*) C. G. Barraclough, R. L. Martin, S. Mitra and R. C. Sherwood, *J. Chem. Phys.*, 1970, **53**, 1638; (*b*) C. G. Barraclough, A. K. Gregson and S. Mitra, *J. Chem. Phys.*, 1974, **60**, 962.

28 (*a*) O. Kahn, *Molecular Magnetism*, VCH, New York, 1993; (*b*) R. L. Carlin, *Magnetochemistry*, Springer, Berlin, 1986; (*c*) C. J. O'Connor, *Prog. Inorg. Chem.*, 1982, **29**, 203.

29 (*a*) B. J. Kennedy and K. S. Murray, *Inorg. Chem.*, 1985, **24**, 1557; (*b*) D. V. Behere and S. Mitra, *Inorg. Chem.*, 1980, **19**, 992.

30 See Ref. 10, p. 174.

31 J. T. Landrum, K. Hatano, W. R. Scheidt and A. C. Reed, *J. Am. Chem. Soc.*, 1980, **102**, 6729.

32 P. Gütlich, H. Köppen, R. Link and H. G. Steinhäuser, *J. Chem. Phys.*, 1979, **70**, 3977.

33 (*a*) B. B. Wayland, L. W. Olson and Z. U. Siddiqui, *J. Am. Chem. Soc.*, 1976, **98**, 94; (*b*) W. M. Coleman and L. T. Taylor, *J. Am. Chem. Soc.*, 1978, **100**, 1075.

34 (*a*) F. A. Cotton and G. Wilkinson, *Advanced Inorganic Chemistry*, 5th edn., Wiley, New York, 1988; (*b*) P. Gouzerh, Y. Jeanin, C. Rocchiccioli-Deltcheff and F. Valentini, *J. Coord. Chem.*, 1979, **6**, 221; (*c*) Y. Sunatsuki, H. Shimada, T. Matsuo, M. Nakamura, F. Kai, N. Matsumoto and N. Re, *Inorg. Chem.*, 1998, **37**, 5566.

35 (*a*) R. Hoffmann and W. N. Lipscomb, *J. Chem. Phys.*, 1962, **36**, 2179; (*b*) R. Hoffmann, *J. Chem. Phys.*, 1963, **39**, 1397.

36 (*a*) K. Tatsumi and R. Hoffmann, *Inorg. Chem.*, 1981, **20**, 3771; (*b*) L. Giannini, E. Solari, S. De Angelis, T. R. Ward, C. Floriani, A. Chiesi-Villa and C. Rizzoli, *J. Am. Chem. Soc.*, 1995, **117**, 5801.

37 (*a*) F. A. Cotton, J. Czuchajowska and X. Feng, *Inorg. Chem.*, 1990, **29**, 4329; (*b*) F. A. Cotton, J. Czuchajowska, L. R. Falvello and X. Feng, *Inorg. Chim. Acta*, 1990, **172**, 135.

38 R. Hoffmann, M. M. Chen, M. Elian, A. R. Rossi and D. M. P. Mingos, *Inorg. Chem.*, 1974, **13**, 2666.

39 K. Tatsumi and R. Hoffmann, *J. Am. Chem. Soc.*, 1981, **103**, 3328.

40 E. Keller, SCHAKAL 88, a FORTRAN Program for the Graphic Representation of Molecular and Crystallographic Models, University of Freiburg, 1988.

Paper a908121f